R04-118

Lebensm.-Wiss. u.-Technol. 37 (2004) 49–58

lwt

www.elsevier.com/locate/lwt

Simulation and verification of ohmic heating in static heater using MRI temperature mapping

Xiaofei Ye[a], Roger Ruan[a,b,c,*], Paul Chen[a], Christopher Doona[d]

[a] *Department of Biosystems and Agricultural Engineering, University of Minnesota, 1390 Eckles Avenue, St. Paul, MN 55108, USA*
[b] *Department of Food Science and Nutrition, University of Minnesota, 1334 Eckles Avenue, St. Paul, MN 55108, USA*
[c] *Nanchang University, Jianxi 330047, China*
[d] *US Army Natick Soldier Center, Combat Feeding Innovative Science Team (Team Leader), Natick, MA 01760, USA*

Received 2 December 2002; accepted 3 June 2003

Abstract

Mathematical modeling of ohmic heating of liquid–particulate mixtures allows insight into the heating behavior, but model verification that uses only a selected number of points in an ohmic heating system is inadequate because of the unknown temperature distribution within the heated food materials, including the locations of hot and cold spots. In this study, ohmic heating of liquid–particulate mixtures was simulated using the finite-element analysis with the commercial software FEMLAB, and the model predictions were verified against temperature maps obtained using magnetic resonance imaging (MRI). A factor ignored by the previous modeling works, the electricity-to-heat conversion efficiency, was considered in the model, resulting in an improved model performance. The electrical conductivity and its temperature dependence for all the materials used in the simulation were determined under consistent electric field strength as the simulated ohmic heating processes. Other factors/parameters affecting model prediction, such as the boundary conditions and heat transfer coefficients, were also determined in situ for an accurate parametric input. The model predictions yielded good agreement with the MRI temperature maps. Results showed that the electrical conductivity of the materials is the most critical factor causing heating rate variations between the particulate phase and the liquid phase. The heating rate variations could be overcome by adjusting the electrical conductivity of the food materials before ohmic heating. This modeling procedure can be used for designing and controlling ohmic heating processes to ensure thermal sterilization and safety of ohmically heated food products.
© 2003 Swiss Society of Food Science and Technology. Published by Elsevier Ltd. All rights reserved.

Keywords: Finite-element analysis; Electricity-to-heat conversion efficiency; Electrical conductivity; Liquid–particulate mixture; PRF; FLASH

1. Introduction

Ohmic heating differs from conventional heating with respect to the heat generation, heat transfer, and temperature distribution patterns occurring during the heating process. Modeling ohmic heating of liquid–particulate mixtures is a difficult task due to the unique characteristics and critical factors that distinguish ohmic heating from conventional heating processes. Independently, controlling the heating rates of the liquid and particulate phases is the key advantage of ohmic heating to ensure uniform sterility in the product, thereby maintaining product quality by reducing over-processing and improving nutrient retention and organoleptic attributes. The rate of heat generation in ohmic heating depends strongly on the electrical conductivity of the food. However, heterogeneous foods (e.g. liquid and particulate food materials may have significantly different electrical conductivity) may exhibit different heat generation rates at distinct localized regions. The consequent heat transfer within a phase or between phases of liquid–particulate mixtures further complicates the determination of temperature distribution in ohmically heated systems. Additional factors contributing to the complexity of the ohmic heating process include possible heat channeling causing hot spots and cold spots, complex coupling between the temperature and electrical fields, and process parameters such as particle size, shape and orientation to the electrical field

0023-6438/$30.00 © 2003 Swiss Society of Food Science and Technology. Published by Elsevier Ltd. All rights reserved.
doi:10.1016/S0023-6438(03)00133-6

(de Alwis, Halden, & Fryer, 1989; Sastry & Palaniappan, 1992a, b).

Understanding the behavior of the ohmic heating process for sterilizing food products is essential for process validation—an actual demonstration of the accurate reliability—and safety of the process (Kim et al., 1996). Mathematical modeling provides insight into the heating behavior of the ohmic processes. The temporal and spatial temperature distribution obtained from a reliable mathematical model can provide information for the calculation of sterility and cook value that will save time and money for validation experiments, and process and product design. Previously proposed models (de Alwis & Fryer, 1990; Sastry & Palaniappan, 1992a, b; Zhang & Fryer, 1993, 1995) to predict temperature distributions under specific heating conditions were experimentally verified with only select points within a system. A continuous spatial verification is needed in order to shed light on the actual temperature distribution. In previous research, we developed (Ye et al., 2003a; Ye, Ruan, Chen, & Doona, 2003b) a noninvasive temperature mapping technique using magnetic resonance imaging (MRI) that enabled fast spatial temperature monitoring during an ohmic heating process without disconnecting the power supply and provided spatial verification of an ohmic heating model.

The performance of a mathematical model for ohmic heating relies in part on accurate inputs of material properties and parameter values. In most (if not all) of the existing models, the electrical conductivity values of both the solid and liquid phases were considered as constants or as linear functions of temperature. Palaniappan and Sastry (1991a, b) showed that the electrical conductivity of a food material is temperature dependent and that it also varies with electrical field strength. Unfortunately, only sparse and inconsistent data are available for this important property (Halden, de Alwis, & Fryer, 1990; Palaniappan & Sastry, 1991a, b; de Alwis & Fryer, 1992). There is a need to investigate this property under a consistent condition as the ohmic heating process. Moreover, an important parameter, the electricity-to-heat conversion efficiency (η), has been ignored in previous modeling work. Preliminary modeling conducted by the authors showed that for a potato–brine mixture heated under 120 V of AC power for 25 min, the temperature at the potato center could be over-predicted by about 25°C if this conversion efficiency was ignored, e.g. assuming the conversion efficiency to be 1 instead of 0.9. By ignoring the conversion efficiency, the electrical energy is assumed convertible to the form of heat completely. But this is impossible in reality because some of the electrical energy, for example, is used to drive the movement of ions. Furthermore, another parameter often simplified or inaccurately estimated in the existing models, the heat transfer coefficient at the liquid–particulate interface, has been investigated using MRI temperature mapping in our previous study (Ye et al., 2003b).

The primary objective of this study was to conduct a three-dimensional simulation of the static ohmic heating of liquid–particulate systems, and to verify the model prediction of the temperature distribution against the temperature maps obtained using MRI temperature mapping. Two reasons support the usefulness of investigating a static ohmic heating system: (a) a near-plug-flow characteristic of foods was demonstrated with high solid content (Zhang et al., 1993); (b) a modified heating section of a ohmic heating system was proposed that could be realized in a positive-displacement plunger-type pump, thus heating could be considered as a semi-batch process. Therefore, it may be that the static simulation condition will yield results that can be directly compared with real continuous system (de Alwis et al., 1990). In order to have accurate parametric inputs to the ohmic model, the following important properties/parameters were also determined: electrical conductivity of liquid and particulate, electricity-to-heat conversion efficiency, and overall heat transfer coefficient at the heating system boundary.

2. Materials and methods

2.1. Materials

The experimental setup for ohmic heating and MRI is shown schematically in Fig. 1.

Two experimental setups were prepared, each consisting of a cylindrical heating device, a potato cylinder, and a salt solution (NaCl) containing sodium carboxymethylcellulose (CMC). The ohmic heating device for sample #1 consisted of a polycarbonate vessel (i.d. = 43 mm) and a nylon stopper at each end. A 40 mm diameter stainless-steel electrode was fixed to each of the stoppers and connected to the power supply. The distance between the two electrodes was 305 mm. A small hole was drilled in the vessel 2 cm off the center lengthwise for injecting the liquid during set up and for releasing pressure during heating. The heating vessel for sample #2 was made of clear PVC tube (i.d. = 63.5 mm) with a 60 mm diameter stainless steel electrode fixed to each of the nylon stoppers of sample #2 and all other dimensions are the same as sample #1. The different sized heating vessels (#1 and #2) served to test the performance of the model under different configurations. The different materials used for the vessels affected the overall heat transfer coefficient at the heater wall.

Two potato cylinders were cut from Russet potato immediately before the experimentation and placed at the center of each heating vessel. The dimension of the potato cylinder was 70 mm (length) × 22 mm (diameter)

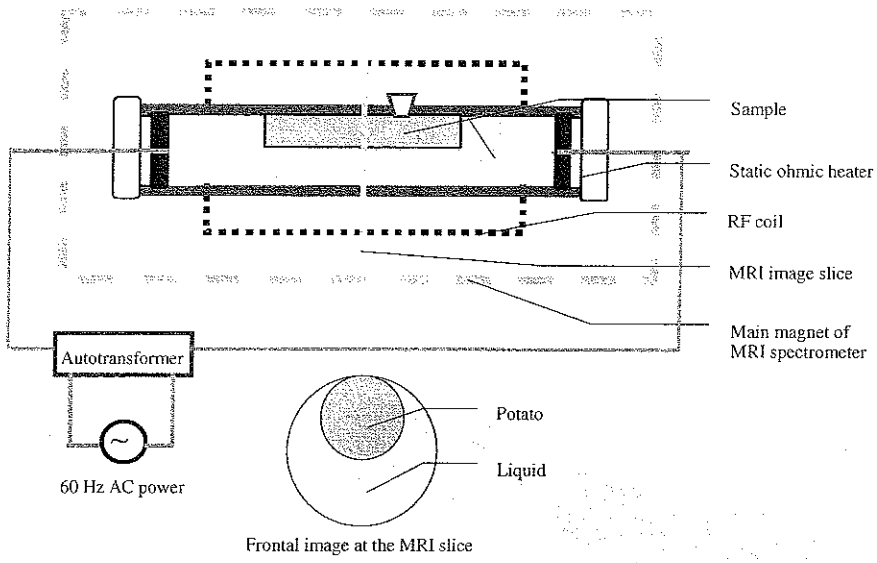

Fig. 1. Schematic diagram of experimental setup.

for sample #1 and 75 mm (length) × 25 mm (diameter) for sample #2. NaCl (S9888, SIGMA®, Sigma-Aldrich Corp.) solutions containing CMC (CEKOL®, Noviant Inc.) were prepared overnight using a hot plate stirrer (Cole-Parmer Instrument Company, Vernon Hills, IL). The CMC and NaCl powders were added gradually to a measured amount of distilled water and heated while being continuously stirred to avoid clumping. For sample #1, the contents of NaCl and CMC were 2 and 10 g/l, respectively. For sample #2, the contents of NaCl and CMC were 5 and 7 g/l, respectively. These contents of salt and CMC were chosen in order to see the effects of salt content and relative viscosity of the liquid on the differential heating between the liquid and solid phases and on the interface heat transfer. The fluid was injected through the small hole into the vessel. Due to the greater density of the solutions, the potato cylinders floated in the fluids, exposing a small portion above the fluid surface because of the leaking of the fluid. The application of an AC power supply through an autotransformer with a constant voltage of 120 V and a frequency of 60 Hz ohmically heated the food systems.

2.2. MR imaging

A volume birdcage radio frequency (RF) coil that fitted the configuration of each heating vessel was used as both an RF transmitter and MR signal receiver. Two-dimensional MR imaging was performed using a 4.7 T SISCO scanner (SISCO, Vermont, CA) with a 400 mm diameter bore at the Center for Magnetic Resonance Research at the University of Minnesota. The proton resonance frequency (PRF) shift method (Ishihara et al., 1995) was incorporated into a fast low-angle shot (FLASH) sequence (Haase, Frahm, Matthaei, Hanicke, & Merboldt, 1986) to achieve a rapid image acquisition. This method exploits the temperature dependence of the water PRF shift (Muller & Reiter, 1965; Hindman, 1966) and the PRF shift can be manifested through MR phase images. Detailed information about the application of the PRF shift method on ohmic heating can be found in Ye et al. (2003a, b). The accuracy of the PRF shift method was calibrated against temperature measurement obtained using fluorescent fiber-optic temperature sensors (Luxtron 750, Luxtron Corp., Santa Clara, CA), and the standard error corresponded to a measurement error of about ±2°C by the PRF shift method.

Transverse images were obtained using the following imaging parameters: repetition time TR = 10 ms; echo time TE = 4.6 ms; flip angle FA ≅ 12°; slice thickness = 3 mm; and image matrix size = 64 × 64. The only difference between the imaging parameters applied to the two samples was the field of view (FOV), which was $60 \times 60\,mm^2$ for sample #1 and $80 \times 80\,mm^2$ for sample #2. Therefore, the temporal resolution (data acquisition time for one temperature map) was 0.64 s for both samples. The spatial resolution of the temperature maps was 0.94 mm for sample #1 and 1.25 mm for sample #2. For sample #1, temperature maps were acquired at 2.5-min intervals for 55 min after turning on the power. For sample #2, temperature maps were obtained every 2.5 min until 25 min after turning on the power.

2.3. Mathematical modeling

Mathematical modeling of the two ohmic heating processes described in the above section was conducted using the software FEMLAB (version 2.2, Comsol Inc., Burlington, MA). FEMLAB uses the finite-element analysis to solve differential equations. The geometry

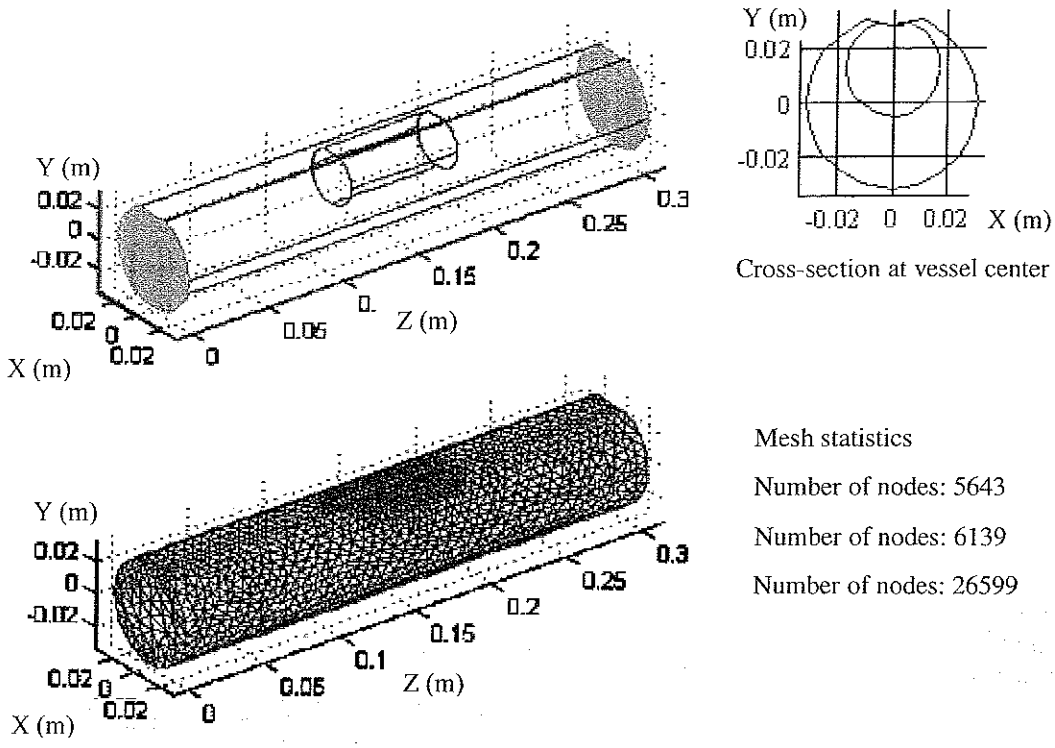

Fig. 2. Geometry and mesh for sample #2 in FEMLAB.

and mesh mode of sample #2 are illustrated in Fig. 2 (and similar to those used for sample #1). A useful feature of FEMLAB is that it can import an MRI image so that we could accurately draw the system geometry; even the leaking of liquid on the top of vessel could be simulated. Two sub-domains (phases), corresponding to the liquid and the potato particulate, were simulated and the AC power was applied through the electrodes in contact with the two ends of the liquid sub-domain (shown in Fig. 2). Adaptive triangular meshing is used by FEMLAB to partition the geometry into tetrahedron elements.

As proposed by de Alwis et al. (1990), the governing equation for electric field is the Laplace equation

$$\nabla \cdot [\sigma_i(T)\nabla V] = 0, \tag{1}$$

in which V represents electric potential, ∇ denotes gradient, $\sigma_i(T)$ designates electrical conductivity of phase i, which has different values for the particulate (p) and liquid (f) phase and varies as a function of temperature (T), thus making the equation system nonlinear. The temperature distribution is determined according to the following equation:

$$\rho_i C_{P_i} \frac{\partial T}{\partial t} = \nabla \cdot (k_i \nabla T) + \dot{u}_i, \tag{2}$$

in which ρ represents the density, C_P the specific heat, t time, and k the thermal conductivity. The symbol $\dot{u}_i$ depicts the internal energy generation by electricity and is defined as

$$\dot{u}_i = \eta |\nabla V|^2 \sigma_i(T), \tag{3}$$

in which η is the electricity-to-heat conversion efficiency. The Neumann boundary condition applies where the liquid surface (s) contacts the vessel wall (w):

$$-k_f \nabla T_f \cdot \vec{n}|_w = U(T_{fs} - T_\infty)|_w \tag{4}$$

and U is the overall heat transfer coefficient at the heater wall. Particulate and liquid temperatures are linked by the convective boundary condition

$$-k_p \nabla T_p \cdot \vec{n}|_s = h_{fp}(T_{ps} - T_f)|_s, \tag{5}$$

in which h_{fp} is the convective heat transfer coefficient at the liquid–particulate interface. The details for estimating h_{fp} was addressed in Ye et al. (2003b), which showed that the h_{fp} varied during ohmic heating holding period. An average value of h_{fp} was used in this study.

The system boundary condition parameter U was estimated in situ according to the following procedure. A solution of viscous brine used in sample #1 or #2 (without particulates) was heated to about 80°C using 120 V, and the applied voltage was decreased to produce a constant temperature of the brine, and the voltage (V) and current (I) data were recorded at an interval of 1 s. The electrical energy input (calculated from numerical integration of the VI vs. t curve) multiplied by η equals the heat loss to the ambient. From the known vessel surface area, U was calculated. The estimation of η and

measurement of electrical conductivity are presented in the next section. Table 1 compiles the material properties and model parameters used for the simulations. The coupled nonlinear partial differential equations (1) and (2) of the electric field and the thermal field with the boundary conditions defined as Eqs. (4) and (5) were solved simultaneously in FEMLAB with a convergence temperature of 0.0001 K.

Table 1
Material properties and parameters used in simulation

Property/parameter	Value for sample #1	Value for sample #2
Diameter of heater vessel (mm)	43	63.5
Length of heater vessel (mm)	305	305
Diameter of potato cylinder (mm)	22	25
Length of potato cylinder (mm)	70	75
Applied voltage V (V)	120	120
Initial temperature (K)	292.2	293
Thermal conductivity of potato k_p[b] (W/m K)	0.571	0.571
Thermal conductivity of liquid k_f[b] (W/m K)	0.612	0.671
Density of potato ρ_p[a] (kg/m^3)	1004	1004
Density of liquid ρ_f[a] (kg/m^3)	1006	1005
Specific heat of potato C_{Pp}[b] (J/kg K)	3515	3515
Specific heat of liquid C_{Pf}[b] (J/kg K)	4050	4050
Overall heat transfer coefficient at heater wall U[c] (W/m^2 K)	25.5	32.4
Liquid-particulate heat transfer coefficient h_{fp}[d] (W/m^2 K)	43.5	59.4
Electricity-to-heat conversion efficiency η[c]	0.85	0.85
Electrical conductivity σ[c]	Function of T	Function of T

[a] Determined in lab by measuring weight and volume.
[b] Rahman, 1995.
[c] Determined in this study.
[d] Ye et al., 2003.

2.3.1. Determination of electrical conductivity and electricity-to-heat conversion efficiency

In this study, all measurements of electrical conductivity were under a field strength same as our ohmic heating experiments (120 V/30.5 cm). A static ohmic heating device similar to the experimental ohmic heater was developed to measure electrical conductivity under ohmic heating conditions. The schematic setup is shown in Fig. 3. This same device was also used to estimate the electricity-to-heat conversion efficiency.

The device consisted of a cylindrical clear PVC sample chamber (i.d. = 23.5 mm) with a stainless-steel electrode at each end and three temperature sensor openings in the chamber. The chamber was thermally insulated by Styrofoam. The distance between the two electrodes was adjustable. Sample liquid or precisely cut potato (cylindrical or rectangular) was placed in the ohmic heating vessel. The applied voltage was adjusted with respect to the sample length to achieve a constant electric field strength (120 V/30.5 cm). Three fluorescent fiber-optic temperature sensors (Luxtron 750, Luxtron Corp., Santa Clara, CA) were inserted into the sample at different locations to monitor local heating rate profiles. Uniform heating in the sample was confirmed by the three temperature readings. Temperature, voltage, and current were continuously recorded on a PC at a constant time interval of 1 s. The electrical conductivity (σ) of samples was calculated based on their dimensions and the voltage and current data as

$$\sigma = L/AR, \tag{6}$$

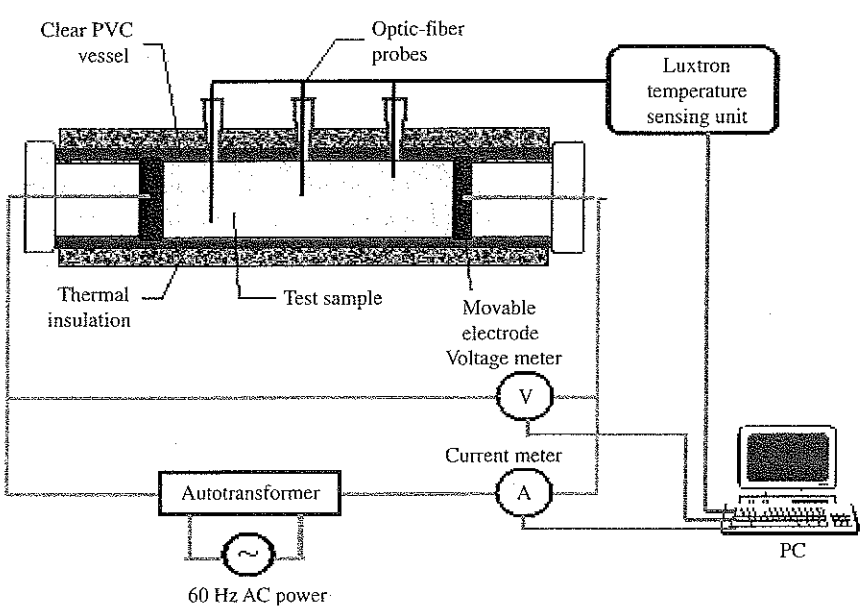

Fig. 3. Schematic setup for measurement of electrical conductivity and estimation of electricity-to-heat conversion efficiency.

in which A is the cross-sectional area of the sample, L is the sample length, and $R = V/I$ the resistance of the sample. Standard NaCl solutions (Cole-Parmer Instrument Company, Vernon Hills, IL) were used to calibrate the device. Reasonable accuracy was achieved (<3%).

The following equation was used to estimate the electricity-to-heat conversion efficiency (η):

$$\eta = \frac{m_1 C_{P1} \Delta T_1 + m_2 C_{P2} \Delta T_2}{\int_0^t VI(t)\,\mathrm{d}t}, \quad (7)$$

in which subscripts 1 and 2 represent the sample and the PVC vessel, respectively, m is the mass, C_P is the specific heat, and ΔT is the temperature change. The numerator of Eq. (7) represents the thermal energy gained by the materials, and the denominator is the input electrical energy.

3. Results and discussion

3.1. Electrical conductivity and electricity-to-heat conversion efficiency

The measurements of σ for NaCl solutions were very reproducible. Determinations of σ for potato, however, produced variations as evident from Fig. 4 that shows five measured replicates. Trials 1a–1c were taken with the same potato sample, and trials 2 and 3 were measured using two different potatoes.

The variation observed for a single potato (trials 1a–1c) was less than that observed for different potatoes. Consequently, the σ data measured from the same single potato as the one used in the ohmic heating experiment were used for the modeling. Importantly, the value of σ (potato) was initially very low, then made a sharp upturn around 320 K, coincident with the gelatinization temperature of potato starch. Fig. 5 gives the $\sigma - T$ data used in the simulation of the two ohmic heating processes. The measurements shown in Fig. 5 for the liquid agree well with the data shown in Kim et al. (1996), in which the σ of 2 and 5.5 g/l salt solution with 55 g/l starch at 19°C were reported as 0.34 and 1.3 S/m, respectively. For the potato particulate, however, discrepancy exists between our measurement (σ(potato) = 0.048 S/m at 19°C) and the data shown in the Kim et al. (σ(potato) = 0.037 S/m at 19°C). The discrepancy might arise from the difference between the applied electric field strength which was not reported in the paper of Kim et al. (1996).

For sample #1, the σ(potato) was initially lower than σ(liquid). As the temperature increased during ohmic heating, the value of σ (potato) eventually exceeded that of σ (liquid). For sample #2, the σ(liquid) showed a higher value than that of the corresponding potato for the entire temperature range of study due to its higher salt content than that for sample#1. Under the applied

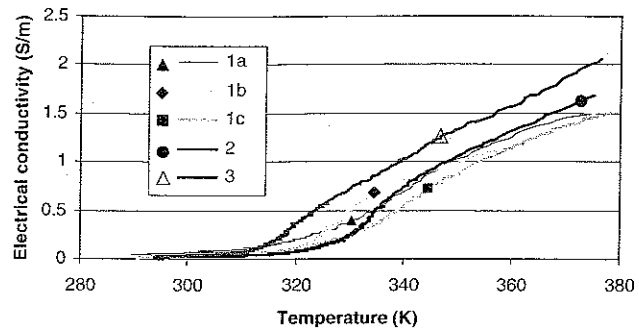

Fig. 4. Five replicates of electrical conductivity measurement for potato.

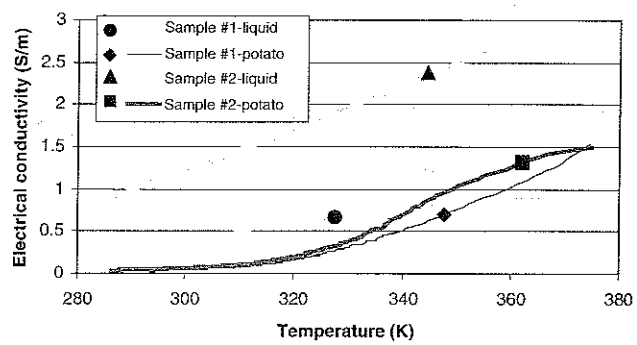

Fig. 5. Electrical conductivity data of the materials used in simulation.

electric field strength, the electrical conductivities of the two solutions exhibited mostly linear functions of temperature, deviating when the temperature approached boiling, whereas the temperature-dependence functions of σ(potato) for each sample were obviously nonlinear. This function was not modeled into a mathematical expression. FEMLAB can take a discrete data table of σ and numerically interpolate (linear interpolation was used in this study) and differentiate it for the iterative calculation, resulting in an accurate input to the modeling.

Twelve samples were tested to estimate values of η, which ranged from 0.78 to 0.85. Considering that it was difficult to account for all the heat loss during the experiments, the highest value of 0.85 was used in the simulation.

3.2. Modeling and MRI verification

The temperature profiles predicted by the model and the corresponding MRI temperature maps at the middle cross section of the ohmic heating systems for selected heating times are presented in Fig. 6 (sample #1) and Fig. 7 (sample #2).

Generally, good agreement between MRI temperature maps and model predictions can be observed.

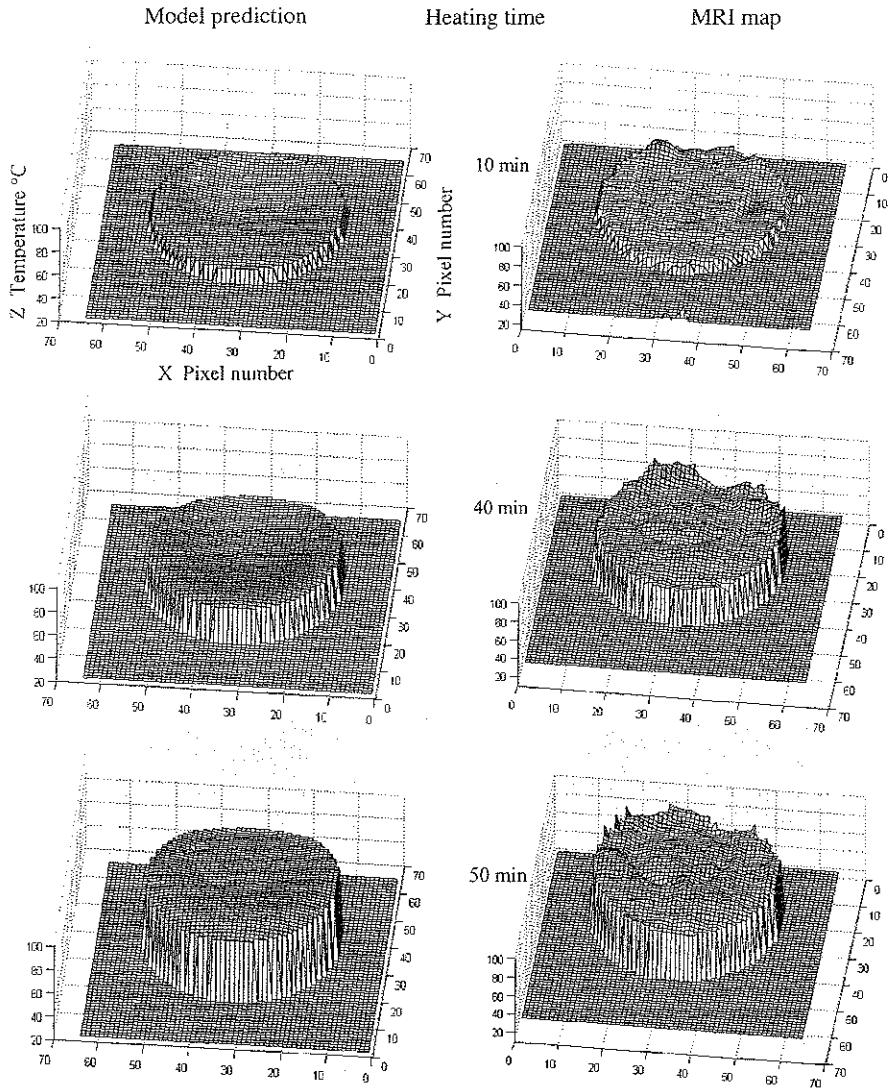

Fig. 6. Model prediction vs. MRI map at middle cross section for sample #1.

Importantly, it can be seen from both the MRI temperature maps and the model predictions that the cold spot in the potato for sample #2 was always located at the center, whereas the cold spot in the potato for sample #1 shifted outward from the center with the ohmic heating progress. This observation shows the importance of the electrical conductivity of the two-phase food materials in determining the location of the cold spot, which is of great concern in the process design. As shown in Fig. 5, the electrical conductivity of the liquid of sample #2, due to its higher salt content comparing with that of sample #1, is much greater than that of the solid through the whole heating range. Therefore, the electrical current was "diverted" through the liquid according to the Laplace equation, resulting in faster heating of the liquid phase in sample #2. Whereas in sample #1, due to the lower salt content of the liquid, the electrical conductivity of potato would catch up with and exceed that of the liquid with the increase of temperature, alleviating or even reversing the current channeling effect in sample #2. The MRI temperature maps provided details of the temperature distribution during ohmic heating, since every pixel in the maps represents a temperature value at that location. Some discrepancies between MRI maps and model predictions should be pointed out. First, the heterogeneous nature of food materials resulted in localized high heating zone and it was difficult to model this phenomena. Second, MRI maps showed sharp transitions at the interface between liquid and potato, while the model predicted smoother transitions, indicating that the interface h_{fp} might still be over-estimated, because the interface heat transfer serves to reduce the temperature difference between the two phases and a larger heat transfer rate would result in smoother transition. Moreover, leaking of liquid from the hole on the top of the heater formed an electrically insulated air zone, complicating the boundary condition in that area and resulting in larger

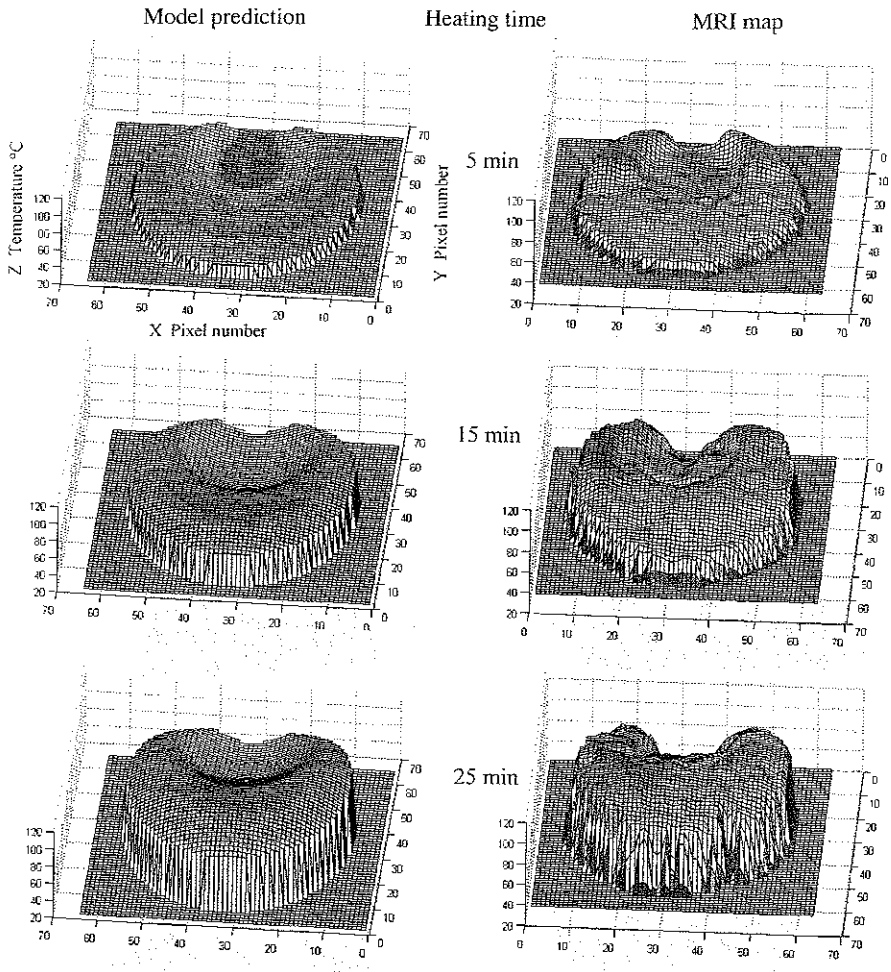

Fig. 7. Model prediction vs. MRI map at middle cross section for sample #2.

difference between MRI maps and model predictions in the area. This is especially obvious for sample #2 in which relatively more liquid leaked out due to the much faster rate of heating and more rapid thermal expansion of this lower relative viscosity solution. It is noteworthy to point out that bubble formation creates electrically insulated zones inside an ohmic heater that detracts from the efficacy of heating and should seriously be considered in heater design and process control to avoid air bubble forming in the heating vessel.

In order to have a closer look at the heating nonuniformity between the two phases, a region of interest (ROI) of 3×3 pixels was extracted from each of potato center and the hotspot in liquid. The hotspots in liquid for the two systems were located between the heater wall and the liquid–particulate interface and were determined as the highest liquid temperature points in the MRI temperature maps at the last heating time. The temperature histories of the average of the ROIs are plotted in Fig. 8 for sample #1 and Fig. 9 for sample #2.

The maximum difference between MRI maps and model predictions during the heating was about 6°C for sample #1 and 8°C for sample #2, indicating a much better agreement compared to previous modeling works, e.g. in a concise review paper of Fu and Hsieh (1999), the difference between the thermocouple measurements and the model predictions could reach as a great value as more than 40°C. Comparing the ROI values from the MRI temperature maps of sample #1 and #2, we can see that the electrical conductivity of the materials was the critical factor affecting heating nonuniformity. For sample #1, the largest temperature difference (about 8°C) between the two phases occurred in the middle of the heating time (≈ 1700 s) and the difference narrowed to about 2°C at the final time point. For sample #2, a wider heating differential between the two phases can be seen, reaching nearly 25°C at the final heating point. The heating nonuniformity in the two samples follows the pattern of the difference between the electrical conductivity of the two phases. The importance of the use of the electricity-to-heat conversion efficiency should be pointed out. We reran the simulation of sample #1 with 100% conversion efficiency ($\eta = 1$ instead of $\eta = 0.85$), and the temperature at the potato center was over-predicted by about 19°C at the last heating point, resulting in a gap as large as 22°C between the

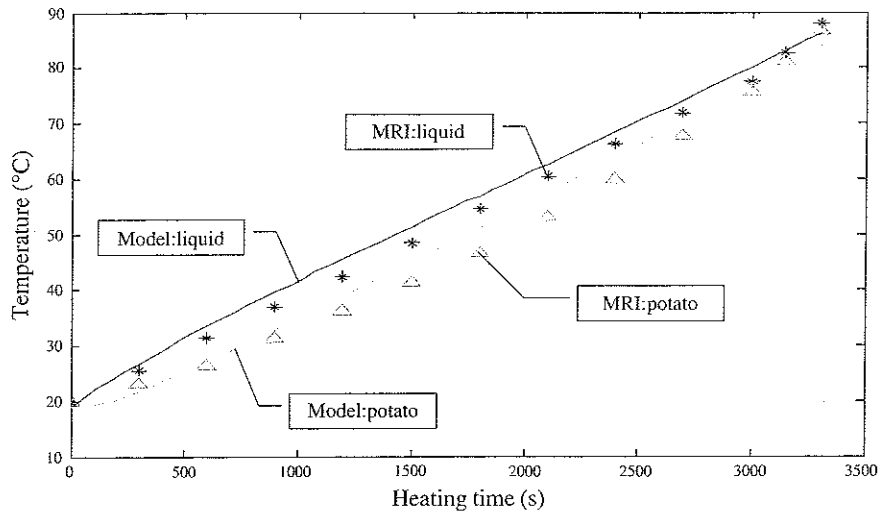

Fig. 8. Temperature history of regions of interest in sample #1 showing heating nonuniformity.

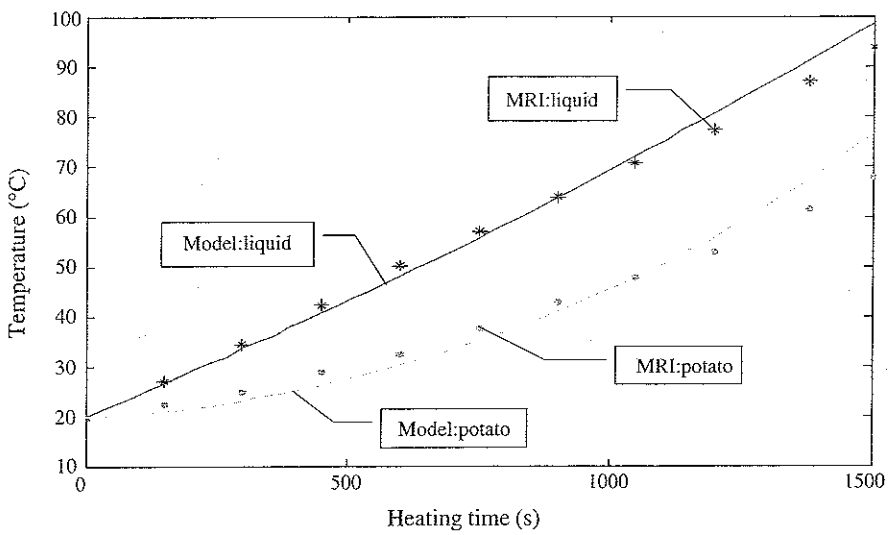

Fig. 9. Temperature history of regions of interest in sample #2 showing heating nonuniformity.

model prediction and the MRI temperature measurement. Other factors, such as density and specific heat, might also be a function of temperature but were simplified as constants in this study. This simplification apparently affected the accuracy of the model prediction. However, the temperature dependence of density or specific heat is a rather weak function. Simulation in FEMLAB using 3650 J/kg K instead of 3515 J/kg K as the value of the potato specific heat resulted in an underprediction of temperature at the center of the potato in sample #1 after 55 min of ohmic heating by only 0.85°C.

4. Conclusions and recommendations

A static ohmic heating process can be simulated if accurate boundary conditions and material properties are provided. The use of the electricity-to-heat conversion efficiency improved the accuracy of the model prediction. The application of the MRI temperature mapping technique provided a detailed verification of the model predictions. The modeling procedure can be used to simulate different heating conditions for process design and control to save time and money. Electrical conductivity of food materials is a crucial factor affecting the heating nonuniformity between the two phases in a liquid–particulate mixture and the heating nonuniformity can be overcome by adjusting the electrical conductivity of the two phases. It is worth studying further to investigate the behavior of electrical conductivity of food materials during ohmic heating. Infusing salt solutions directly into the potato would change the electrical conductivities of the potatoes and impact the observed heating patterns, including the possibility of heating the potato particulate faster than the NaCl solution under appropriate circumstances. The

configuration of the ohmic heating processes simulated in this study represents the worst-case scenario that can be used to ensure the safety of the processed products. Future research can add in the Navier–Stokes equation for fluid flow to be solved together with the thermal field and the electric field equations in order to simulate a continuous ohmic heating process. Meanwhile, a development of MRI temperature mapping technique for flowing materials is needed for the modeling guidance and verification.

References

de Alwis, A. A. P., & Fryer, P. J. (1990). A finite element analysis of heat generation and transfer during ohmic heating of foods. *Chemical Engineering Science*, *45*, 1547–1559.

de Alwis, A. A. P., & Fryer, P. J. (1992). Operability of the ohmic heating process: Electrical conductivity effects. *Journal of Food Engineering*, *15*(1), 21–48.

de Alwis, A. A. P., Halden, K., & Fryer, P. J. (1989). Shape and conductivity effects in the ohmic heating of foods. *Chemical Engineering Research Design*, *67*, 159–168.

Fu, W. R., & Hsieh, C. C. (1999). Simulation and verification of two-dimensional ohmic heating in static system. *Journal of Food Science*, *64*(6), 946–949.

Haase, A., Frahm, J., Matthaei, D., Hanicke, W., & Merboldt, K. D. (1986). FLASH imaging: Rapid NMR imaging using low flip-angle pulse. *Journal of Magnetic Resonance*, *67*, 258–266.

Halden, K., de Alwis, A. A. P., & Fryer, P. J. (1990). Changes in the electrical conductivity of foods during ohmic heating. *International Journal of Food Science and Technology*, *25*(1), 9–25.

Hindman, J. C. (1966). Proton resonance shift of water in the gas and liquid states. *Journal of Chemical Physics*, *44*, 4582–4592.

Ishihara, Y., Calderon, A., Watanabe, H., Okamoto, K., Suzuki, Y., Kuroda, K., & Suzuki, Yu. (1995). A precise and fast temperature mapping using water proton chemical shift. *Magnetic Resonance in Medicine*, *34*, 814–823.

Kim, H. J., Choi, Y. M., Yang, T. C. S., Taub, I. A., Tempest, P., Skudder, P., Tucker, G., & Parrott, D. L. (1996). Validation of ohmic heating for quality enhancement of food products. *Food Technology*, *50*(5), 253–255, 257–261.

Muller, N., & Reiter, R. C. (1965). Temperature dependence of chemical shifts of protons in hydrogen bonds. *Journal of Chemical Physics*, *42*, 3265–3269.

Palaniappan, S., & Sastry, S. K. (1991a). Electrical conductivities of selected solid foods during ohmic heating. *Journal of Food Process Engineering*, *14*(3), 221–236.

Palaniappan, S., & Sastry, S. K. (1991b). Electrical conductivities of selected juices: Influences of temperature, solid content, applied voltage, and particle size. *Journal of Food Process Engineering*, *14*(3), 247–260.

Rahman, S. (1995). *Food properties handbook*. Boca Raton, FL, USA: CRC Press.

Sastry, S. K., & Palaniappan, S. (1992a). Influence of particle orientation on the effective electrical resistance and ohmic heating rate of a liquid–particle mixture. *Journal of Food Process Engineering*, *5*(3), 213–227.

Sastry, S. K., & Palaniappan, S. (1992b). Mathematical modeling and experimental studies on ohmic heating of liquid–particle mixtures in a static heater. *Journal of Food Process Engineering*, *15*(4), 241–261.

Ye, X., Ruan, R., Chen, P., Chang, K., Ning, K., Taub, I., & Doona, C. (2003a). Accurate and fast temperature mapping during ohmic heating using PRF shift MRI thermometry. *Journal of Food Engineering*, *59*(2–3), 143–150.

Ye, X., Ruan, R., Chen, P., Doona, C., & Taub, . I. (2003b). MRI temperature mapping and determination of the liquid–particulate heat transfer coefficient in an ohmically heated food system. *Journal of Food Science*, *68*(4), 1341–1346.

Zhang, L., & Fryer, P. J. (1993). Models for the electrical heating of solid–liquid food mixtures. *Chemical Engineering Science*, *48*, 633–643.

Zhang, L., & Fryer, P. J. (1995). A comparison of alternative formulations for the prediction of electrical heating rates of solid–liquid food materials. *Journal of Food Process Engineering*, *18*, 85–97.